[CANCER RESEARCH 63, 3646–3653, July 1, 2003]

# Enhanced Tumor Suppression by a p14ARF/p53 Bicistronic Adenovirus through Increased p53 Protein Translation and Stability[1]

**Yinghui Huang, Traci Tyler, Neshat Saadatmandi, Casey Lee, Per Borgstrom, and Ruth A. Gjerset[2]**

*Sidney Kimmel Cancer Center, San Diego, California 92121*

## ABSTRACT

**The p53 tumor suppressor controls a cell cycle arrest and apoptosis pathway that is central to tumor suppression and often disrupted in cancer. The accumulation and activity of p53 are positively controlled by the p14 ADP p14ARF ribosylation factor (AR) tumor suppressor, and full restoration of the pathway in cancer cells may require that both p53 and p14ARF be supplied. To address this issue, we have constructed a bicistronic adenoviral vector encoding the two proteins (Adp14/p53) and compared its tumor suppressor activity with that of a single gene vector for p53 (Adp53). We find that tumor cells treated with Adp14/p53 undergo a much sharper decrease in viability with increasing multiplicities of infection than do cells treated with Adp53, even when cells express endogenous p14ARF. Adp14/p53 is also more effective than is a combination of single gene vectors for p14 and p53. The sharper decrease in cell viability after treatment of cells with Adp14/p53 correlates with an increased rate of p53 protein synthesis and a decreased rate of p53 protein turnover, leading to increased steady-state levels of p53 protein and increased levels of p53 downstream targets mdm2, p21waf1, and bax. Adp14/p53 treatment leads to an elevated bax:bcl2 ratio and induction of apoptosis *in vitro* and *in vivo*, coupled with a failure of the tumor cells to induce neovascularization *in vivo*. The results indicate that endogenous p14ARF expression may be insufficient to ensure efficient accumulation of ectopic p53 after gene transfer and demonstrate that for tumor suppression, bicistronic coexpression of p14ARF and p53 is superior to p53 alone. The results show that in this setting, p14ARF promotes p53 accumulation by increasing p53 protein synthesis, in addition to its well-characterized ability to oppose mdm2-mediated degradation of p53.**

## INTRODUCTION

The p53 tumor suppressor controls a key cell cycle arrest and apoptosis pathway that is central to tumor suppression. The pathway is triggered through stabilization of the p53 protein and activation of its transcriptional transactivation properties in response to a variety of cellular abnormalities commonly found in cancer, including oncogene expression and DNA damage. One of the transcriptional targets of p53 is mdm2, a p53-binding protein and important negative regulator of p53 (1). Binding of mdm2 to p53 is disrupted after DNA damage (2), and this disables negative regulation of p53 by mdm2 and promotes the accumulation of p53 protein. Recently, mdm2 has been found to play a dual role in the regulation of p53, promoting increased translation of p53, as well as degradation of p53 protein (3). An important positive regulator of p53 is p14ARF, an mdm2-binding protein that opposes the activity of mdm2 and is induced in response to oncogenes (4, 5). p53, in turn, suppresses the *p14ARF* promoter (6). Together, p53, mdm2, and p14ARF act in a regulatory feedback loop that maintains low-level expression of p53 under normal conditions, while enabling a rapid accumulation of p53 in response to DNA damage or oncogene activation.

Abrogation of the p53 pathway is probably common to most cancers and may therefore be an essential step in tumor development, with loss or mutation of the *p53* gene occurring in some 50–60% of cancers overall (7, 8). *p14ARF* gene loss has often been found to occur in a reciprocal manner to *p53* loss and may account for most cancers that retain wild-type *p53* (9, 10). Overexpression of mdm2 occurs in a variety of cancers with less frequency and may account for some 10% of cancers overall (11). Ectopic overexpression of wild-type p53 restores the pathway, in whole or in part, and is highly suppressive of growth and viability of a wide variety of tumor cell types but is minimally suppressive of normal cells (12, 13). For this reason, the p53 pathway has attracted attention not only for its importance to cancer cell biology but also for its potential for cancer treatment (14).

The fact that p53 is regulated by activation signals, such as DNA damage, and regulatory proteins, such as p14ARF and mdm2, may explain why permanent cell cycle arrest or apoptosis is not always achieved in tumor cells by ectopic overexpression of p53 alone. In some cases, a greater apoptotic response has been achieved if ectopic expression of p53 is combined with a treatment that promotes DNA damage, such as cisplatin (13, 15), UV or ionizing radiation (16), or inhibition of DNA repair (12, 17). Clinically, this observation has translated into combination therapies involving a p53 adenovirus together with a DNA-damaging therapy, such as cisplatin or radiation, and improved antitumor responses have been observed compared with single agent treatments (14).

The activity of ectopically expressed p53 is also subject to attenuation by the p53/mdm2/p14ARF[3] feedback loop, which provides a mechanism whereby p53 down-regulates its own expression through induction of mdm2. Certain cancer-associated abnormalities, such as overexpression of mdm2 or loss of p14ARF, would tend to exacerbate this effect, creating an even greater obstacle to high-level accumulation of p53 after p53 gene transfer. Full restoration of the p53 pathway is therefore likely to require additional steps to modulate the feedback loop or activate p53.

To examine how coexpression of p14ARF and p53 affects p53-mediated tumor suppression, we have used a bicistronic adenoviral vector that provides high-level ectopic expression of both proteins. We find that bicistronic coexpression of p14ARF and p53 greatly enhances the synthesis and accumulation of p53 protein and leads to a dramatic enhancement in tumor suppression relative to p53 alone. The results have bearing on the regulation of p53 by p14ARF, as well as on the eventual clinical application of *p53* gene transfer for the treatment of cancer.

## MATERIALS AND METHODS

**Cell Lines.** DLD-1 human colon cancer cells were obtained from the American Type Culture Collection (Rockville, MD). Murine N202 cells, which overexpress the rat neu proto-oncogene driven by the mouse mammary tumor

Received 11/27/02; accepted 5/1/03.

The costs of publication of this article were defrayed in part by the payment of page charges. This article must therefore be hereby marked *advertisement* in accordance with 18 U.S.C. Section 1734 solely to indicate this fact.

[1] Supported in part by grants (to R. A. G.) from the California Cancer Research Program 99-00517V-10140, the California Breast Cancer Research Program 6JB-0077, the Tobacco Related Disease Research Program 11RT-0074, the Department of Defense Breast Cancer Research Program DAMD 17-96-1-6038, the National Cancer Institute CA69546, and a Research Agreement with Introgen Therapeutics, Inc. (Houston, TX).

[2] To whom requests for reprints should be addressed, at Sidney Kimmel Cancer Center, 10835 Altman Row, San Diego, CA 92121. E-mail: rgjerset@skcc.org.

[3] The abbreviations used are: ARF, alternate reading frame; ADP ribosylation factor; CMV, cytomegalovirus; pfu, plaque-forming unit(s); m.o.i., multiplicities of infection; GFP, green fluorescent protein; FACS, fluorescence-activated cell sorter; RT-PCR, reverse transcriptase-PCR.

virus promoter/enhancer (18), were kindly provided by Dr. Joseph Lustgarten (Sidney Kimmel Cancer Center). Cell lines were maintained at 37°C in 10% $CO_2$ in DMEM supplemented with nonessential amino acids, pyruvate, L-glutamine, gentamicin, and 10% heat-inactivated fetal bovine serum (all obtained from Irvine Scientific, Santa Ana, CA).

**Adenoviral Vectors.** A replication defective adenoviral vector, deleted in E1A, E1B, and E3, was constructed in which the viral *E1A* and *E1B* genes were replaced with a bicistronic cassette encoding *p14ARF* and *p53* under the control of the CMV promoter, using the AdEasy vector system (Quantum Biotechnologies), following the manufacturer's protocol. The bicistronic cassette was obtained from the pIRES vector of Clontech, Inc. (Carlsbad, CA). The *p53* coding sequence was placed downstream of the internal ribosome entry site. An Adenoviral vector encoding p14ARF was prepared similarly except that the coding sequence for *p14ARF* was directly inserted into the multicloning site of pSHUTTLE-CMV. Viral packaging and expansion were accomplished by transfection of human kidney 293 cells (QBI-293A cells; Quantum Biotechnologies). Virus was purified from cell lysates using a ViraPur column (ViraPur, LLC, Carlsbad, CA, now marketed through BD Biosciences Clontech, Palo Alto, CA). Viral titers (pfu/ml) were determined by the tissue culture infectious pose 50 assay described in the Quantum Biotechnologies AdEasy applications manual and were in the range of $10^9$-$10^{10}$ pfu/ml. Replication-defective adenoviral vectors encoding human wild-type p53 (INGN201, Ad5CMV-p53), bacterial β-galactosidase, and firefly luciferase were provided by Introgen Therapeutics, Inc. (Houston, TX). These are referred to here as Adp53, Adβ-gal, and AdLuc, respectively. The *p53* and *β-galactosidase genes* are expressed from the CMV promoter. The *luciferase* gene is expressed from the Rous Sarcoma Virus promoter. Viral titers are as follows: (*a*) Adp53: $3.6 \times 10^{10}$ pfu/ml; (*b*) Adβ-gal: $2.4 \times 10^{10}$ pfu/ml; and (*c*) AdLuc: $2 \times 10^{11}$ pfu/ml.

**Growth and Viability Assays.** Cells at 60–70% confluency in 24-well plates were treated with adenoviral vectors in medium containing 2% fetal bovine serum at various m.o.i. for 4 h and then replated in triplicate in 96-well plates at 2000 cells/well in complete medium. Under these conditions, control (untreated) wells remained subconfluent and in exponential phase growth for the duration of the assay. After 72 h, viability was determined by the bioconversion of (3-(4,5′-dimethylthiazol-2-yl)-5-(3-carboxymethoxylphenyl-2-(4-sulfophenyl)-2H-tetrazolium(3-(4,5′-dimethylthiazol-2-yl)-5-(3-carboxymethoxylphenyl-2-(4-sulfophenyl)-2H-tetrazolium inner salt; Promega Corp., Madison, WI) to a colored product, measured by absorbance at 490 nm as described previously (19). Viability was expressed as a percentage of uninfected cell viability.

**RT-PCR.** Gene expression analyses were carried out 24- or 48-h postvector treatment. Total cellular RNA was prepared from ~$10^6$ cells using the RNeasy mini kit from Qiagen, Inc. (Valencia, CA), reverse transcribed into cDNA, and amplified by PCR (under linear conditions) as described previously (19). Control cDNA reactions lacking reverse transcriptase produced no band on PCR amplification, indicating the absence of genomic DNA sequences. Primers were chosen so as to amplify a 200–300 base fragment of the gene and synthesized by Sigma Genosys. PCR products were analyzed by agarose gel electrophoresis, and bands were quantitated using Kodak digital camera and analysis software.

**Western Analysis.** A cell lysate (10–30 μg) was analyzed by Western analysis as described previously (20). Mouse monoclonal panspecifc antihuman p53 (Clone DO-1, Ab-6) and mutant-specific anti-p53 (Clone PAb 240, Ab-3) were purchased from Oncogene Research Products (Cambridge, MA) and used at 1:500. Rabbit polyclonal anti-$p14^{ARF}$ (full-length protein) was purchased from Zymed Laboratories, Inc. (South San Francisco, CA) and used at 1:500. Mouse monoclonal anti-mdm2 (human) SMP14 (used at 1:100), rabbit polyclonal anti-bax (used at 1:200), rabbit polyclonal anti-$bcl_2$ (used at 1:100), mouse monoclonal anti-actin (used at 1:500), and horse radish peroxidase conjugated antirabbit and antimouse secondary antibodies (used at 1:1000) were purchased from Santa Cruz Biotechnologies, Inc. (Santa Cruz, CA). Antibody reactive bands were revealed using the ECL+Plus Western blotting detection system (Amersham Life Sciences, Little Chalfont, Buckinghamshire, England, United Kingdom). For quantitation of bands, we used Kodak digital camera and analysis software.

**Radioactive Pulse, Pulse Chase, and Immunoprecipitation.** Cells were grown in 3.5-cm culture dishes, treated with the indicated vector doses (as described above), and labeled 24-h postvector treatment in methionine/cysteine-free medium (ICN) supplemented with 10% dialyzed FBS and 100 μCi $^{35}$S-methionine (ICN; 10 mCi/mmol) for 1 h. Labeling medium was then removed, and cells were washed with complete growth medium. Cells were harvested at the indicated times, lysed in 400 μl of buffer, and subjected to immunoprecipitation as described previously (21), using 10 μl of pan-specific antihuman p53 [mouse monoclonal, Ab-6 (Clone DO-1), see above] plus 30 μl of protein G-agarose (Santa Cruz Biotechnologies, Inc.) overnight at 4°C with rotation. Immunoprecipitates (20 μg of equivalents of original cell lysates) were analyzed by SDS-PAGE followed by fluorography (21). To clear endogenous mutant p53 from DLD-1 cell lysates, samples were subjected to two serial pretreatments for 2 h each with rotation at 4°C with 10 μl of mutant-specific anti-p53 [mouse monoclonal Ab-3 (Clone PAb 240) see above] plus 30 μl of protein G-agarose, before treating lysates with panspecifc antihuman p53 (DO-1). Bands corresponding to p53 were quantitated using Kodak digital camera and analysis software, and protein half-life was calculated based on the formula $n_t = n_o 2^{rt}$, where $n_o$ and $n_t$ are the band intensities at time 0 and time t after the pulse, and r is the rate of decay.

**Animal Chamber Model.** Dorsal skinfold chambers in female nude mice (20–25 grams of body weight) were prepared according to a method described previously (22). Intravital microscopy was performed using a Mikron fluorescence microscope (Mikron Instruments, San Diego, CA; Ref. 23). For the visualization of nuclear events, cells were transduced with retroviral vectors encoding a histone H2B-GFP fusion gene (construct kindly provided by Drs. Teru Kanda and Geoffrey Wahl; Salk Institute, La Jolla, CA). To prepare spheroids, N202-H2B-GFP cells were plated in 24-well plates and treated with 20 pfu/cell AdLuc (control), Adp53, or Adp14/p53 for 4 h as described in the growth and viability assays. Immediately after vector treatment, tumor cell spheroids were prepared as described previously (19). Later (36 h), spheroids were removed from 96-well plates and implanted into the dorsal skin fold chamber of nude mice as described previously (23). Cell viability was visualized by the intrinsic fluorescence of H2B-GFP. Visualization of mitotic activity and nuclear fragmentation and condensation characteristic of apoptotic cells were carried out under ×40 and ×63 objectives. Autofluorescence was minimized by using a narrow band filter set 31026 (Chroma, Brattleboro, VT). Where visualization of vasculature was needed, the images (×4) were obtained using a BG12 filter for RBC enhancement and Retinex Image Enhancement, a method of improving the dynamic range compression, color constancy, and color retention for a digital image (PhotoFlair; True View Imaging Co., Hampton, VA). Tumor growth based on the total intensity, $I_T$, of GFP fluorescence, was determined using the formula:

$$I_T = \sum_{k=75}^{255} kN_k$$

where $N_k$ is the number of pixels with photo intensity k (within the gray level range of 75–255). The photo intensity, k, is again introduced as a correction factor to account for the fact that cell density increases with increasing photo density and that pixels with greater photo density should be weighted more heavily. A standard curve relating $I_T$ to number of tumor cells was constructed by implanting spheroids containing known numbers of H2B-GFP-expressing N202 cells into chambers, determining $I_T$, and applying a quadratic curve fitting algorithm.

**Trypan Blue Exclusion Assay of Membrane Permeability.** Duplicate wells of cells in 24-well plates were treated with vector as described above and assayed 48-h postvector treatment for Trypan Blue uptake as described previously (19).

**Cell Cycle and Apoptosis Analysis.** Cell cycle and apoptosis analysis were performed on propidium iodide-stained cells as described previously (13) using a FACScan Flow cytometer (Becton Dickinson, Franklin Lakes, NJ). DNA histograms were analyzed with the ModFit program using doublet discrimination. Each analysis was performed in duplicate.

## RESULTS

**Adp14/p53 Induces Greater Accumulation of p53 Protein than Does Adp53.** We examined expression of the *p53* and *p14ARF* genes in human DLD-1 colon cancer cells (endogenous mutant p53) and

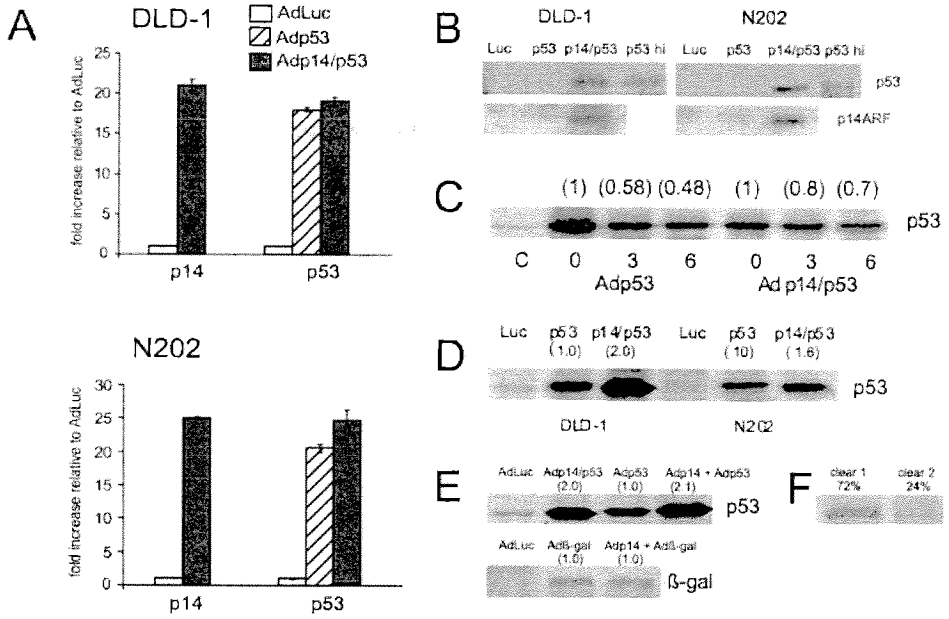


Fig. 1. *A*, semiquantitative RT-PCR analysis of vector-induced expression of human p14ARF and p53 RNA 24 h after treatment of N202 and DLD-1 cells with 20 pfu/cell AdLuc, Adp53, or Adp14/p53 for 4 h. Bars represent averages of triplicate samples with SD shown. *B*, Western analysis of p53 and p14ARF protein expression 48 h after the same treatments as in *A*. In addition, in the case of p53, an additional sample treated with 200 pfu/cell Adp53 (*p53 hi*) is included. Endogenous p53 protein was immunodepleted from DLD-1 cell lysates before Western analysis. Each *lane* represents 10 μg of protein for the p53 analysis and 30 μg of protein for the p14ARF analysis. *C*, $^{35}$S-methionine pulse chase experiment followed by immunoprecipitation of p53 carried out on cells 24 h after vector treatment as in *A*. Endogenous mutant p53 in DLD-1 cells was precleared before immunoprecipitation of ectopic wild-type p53. Each *lane* represents the equivalent of 20 μg of initial lysate protein. Numbers above the *lanes* represent p53 band intensities relative to time 0, determined by digital analysis. Numbers below *lanes* indicate length of chase time (in h) after the 1-h pulse. Control lane (*c*) represents uninfected cells. *D*, immunoprecipitated p53 immediately after a 1-h $^{35}$S-methionine pulse of cells treated with vector as in *A*. Each *lane* represents the equivalent of 20 μg of initial lysate protein. Numbers above *lanes* represent band intensities relative to p53 lane. *E*, immunoprecipitated p53 immediately after a 1-h $^{35}$S-methionine pulse of cells treated with vector as in *A*. For combination treatments, cells received 20 pfu/cell Adp53 + 20 pfu/cell Adp14 or 100 pfu/cell Adβ-gal + 20 pfu/cell Adp14. Each *lane* represents the equivalent of 20 μg of initial lysate protein. Numbers above *lanes* represent band intensities relative to p53 lane. *F*, preclearing results showing two serial immunoprecipitations of endogenous p53 (using mutant-specific pAb240) from AdLuc-treated cells immediately after the 1-h $^{35}$S-methionine pulse.

murine N202 cells (endogenous wild-type p53)[4] after treatment with 20 pfu/cell AdLuc (control), Adp53, or bicistronic Adp14/p53. Both cell lines express endogenous p14ARF based on RT-PCR analysis.[4] The p53 pathway is highly conserved in humans and rodents, permitting human p53 to replace rodent p53 as a tumor suppressor in rodent systems (24). Furthermore, although human and mouse p53 share extensive homology, they can be distinguished immunologically using the DO-1 human-specific antibody. In the case of DLD-1 cells, endogenous mutant p53, which accounted for some 10–20% of total p53 after the treatment of cells with 20 pfu/cell Adp14/p53 or Adp53, respectively (based on a radioactive pulse experiment; data not shown), was precleared from cell lysates as described (see "Materials and Methods"). More than 90% of endogenous mutant p53 could be cleared through two serial preclearings (Fig. 1*F*).

Semiquantitative RT-PCR analysis of *p14ARF* and *p53* gene expression in N202 and DLD-1 cells 24 h after treatment with 20 pfu/cell AdLuc (control), Adp14/p53, or Adp53 demonstrated that Adp14/p53 induced equivalent levels of *p14ARF* and *p53* at the level of message and that Adp14/p53 and Adp53 induced equivalent levels of *p53* message (Fig. 1*A*). Under the conditions used to measure levels of ectopic message, endogenous message was barely detectable, and levels in untreated cells (data not shown) were similar to levels after treatment with AdLuc. Expression of p14ARF and p53 protein was analyzed by Western analysis 48 h following the same vector treatments (Fig. 1*B*). In addition, a sample treated with 200 pfu/cell Adp53 was included for p53 analysis (p53 hi). Endogenous p14ARF protein was undetectable in both cell lines under our Western analysis conditions, but ectopic p14ARF was clearly induced after treatment with Adp14/p53. Endogenous p53 was also undetectable under our Western conditions, even in DLD-1 cells before preclearing (data not shown). In the case of ectopic p53, a digital analysis of p53 bands in a darker exposure revealed a 16- and 13-fold difference in p53 band intensities between Adp14/p53- and Adp53-treated samples in DLD-1 and N202 cells, respectively. Furthermore, p53 band intensities in samples from Adp14/p53-treated cells (20 pfu/cell) were some 2-fold stronger than in samples from p53 hi-treated cells (200 pfu/cell), consistent with the greater biological effect of Adp14/p53 (see below). Because the Adp14/p53 and Adp53 vectors produced similar levels of *p53* message when each was administered at 20 pfu/cell (Fig. 1*A*), the results suggest the involvement of post-transcriptional or post-translational controls over protein accumulation.

Because p14ARF is known to oppose mdm2-mediated ubiquitination and degradation of p53, we examined p53 protein half-life after treatment with Adp14/p53 or Adp53. The stability of the p53 protein was evaluated by carrying out a pulse chase experiment with $^{35}$S-methionine 24 h after treatment of DLD-1 cells with either Adp14/p53 (20 pfu/cell) or Adp53 (200 pfu/cell; Fig. 1*C*), treatment conditions that achieve roughly equivalent steady-state levels of transduced p53 for the two vectors. The results showed that the intensity of labeling of ectopic p53 decreased more rapidly during the chase period in cells treated with Adp53 than it did in cells treated with Adp14/p53 (Fig. 1*C*). The fractional remaining radioactivity in p53 relative to time 0, as determined by Kodak digital analysis of band intensities, is indicated above each lane in Fig. 1*C*, and was used to calculate p53 half-life. The calculated half-life of ectopic wild-type p53 protein in vector-treated cells was 4.1 ± 2.2 h for Adp53-treated cells and 10.5 ± 1.7 h for Adp14/p53-treated cells. An independent repeat experiment produced similar results.

[4] Y. Huang and R. A. Gjerset, unpublished observations.

Not only did p53 protein half-lives differ after treatment with Adp53 or Adp14/p53, but synthesis rates differed as well. At equal m.o.i. for the two vectors (20 pfu/cell), where message levels for *p53* were similar (Fig. 1*A*), Adp14/p53 treatment resulted in some 2-fold higher levels of incorporation of $^{35}$S-methionine into p53 protein after a 1-h pulse (Fig. 1*D*). This observation was repeated in a second independent experiment. Differences in p53 half-life would contribute negligibly to differences in band intensities in this timeframe and could not account for the differences observed. An effect of p14ARF on p53 protein synthesis rates was also seen in cells treated with a combination of single gene vectors, Adp53 and Adp14, each at 20 pfu/cell (Fig. 1*E*). Furthermore, although incorporation of $^{35}$S-methionine into p53 increased in cells treated with Adp14/p53 or Adp14 + Adp53, overall incorporation into total cellular protein decreased by 20 and 7%, respectively, relative to cells treated with AdLuc or Adp53 (data not shown). Finally, when cells were treated with a combination of Adp14 (20 pfu/cell) together with Ad$\beta$-gal (100 pfu/cell), a vector similar to Adp53 in which the bacterial *β-galactosidase* gene replaces p53, we observed no effect of p14ARF expression on incorporation of $^{35}$S-methionine into β-galactosidase (Fig. 1*E*). Taken together, these results indicate that observed effects of p14ARF on p53 synthesis are vector independent and p53 specific.

**Adp14/p53 Displays Enhanced Tumor Suppressor Activity *in Vitro* Relative to Adp53.** We examined the *in vitro* tumor suppressor activity of Adp14/p53 relative to Adp53 in DLD-1 and N202 cells using 72-h viability assays as described in "Materials and Methods." In both DLD-1 and N202 cells, Adp14/p53 was far more suppressive of growth than was Adp53, achieving complete suppression at m.o.i. of 20 and 50 pfu/cell, respectively, some 20-fold less than doses needed of Adp53 to achieve similar effects (Fig. 2, *A* and *B*). Adp14/p53 was also more effective than was a combination of single gene vectors for p53 and p14ARF (Fig. 2*C*), suggesting that the bicistronic vector was far more efficient at achieving uniform coexpression of the two genes throughout the cell population.

Suppression of growth after treatment with Adp14/p53 correlated with increased cell death, as determined by a Trypan Blue exclusion assay of cellular membrane permeability. Fig. 2*D* plots the results of Trypan Blue staining carried out 48 and 72 h after treatment of DLD-1 or N202 cells with AdLuc, Adp53, or Adp14/p53 at 20 pfu/cell, as well as Adp53 at 200 pfu/cell. All cells, including adherent and floating cells, were scored, and bars represent the average of duplicate treatments. In the case of Adp14/p53, cell death (Trypan Blue-positive cells) reached a high level by 72-h post-treatment and accounted for some 95 ± 1% (DLD-1) and 84.5 ± 1% (N202) of the cells, consistent with the marked reduction in cell viability relative to control observed at 72 h (Fig. 2, *A* and *B*). In the case of Adp53 at 20 pfu/cell, cell death relative to control (AdLuc) remained low even at 72-h post-treatment and accounted for some 2 ± 1% (DLD-1) and 25 ± 3% (N202), consistent with the minimal reduction in cell viability relative to control observed at 72 h after this treatment (Fig. 2, *A* and *B*). Background levels of cell death were undetectable for DLD-1 and 8 ± 4% for N202. At a treatment dose of 200 pfu/cell, Adp53 higher levels of Trypan Blue staining were observed and accounted for some 42 ± 14% (DLD-1) and 39 ± 5% (N202) of the treated cells. Because overall suppression of viability relative to control was observed to be >60% at this treatment dose (Fig. 2, *A* and *B*), cell cycle arrest without cell death may also contribute to the suppression of viability by high-dose Adp53 in this setting.

Cell cycle changes and apoptosis were evaluated by FACS analysis of propidium iodide-stained cells 48 h after treatment with 20 pfu/cell the various vectors (Fig. 2*E*). We found that Adp53 treatment of DLD-1 and N202 cells at this dose had little effect on the overall cell cycle distribution compared with AdLuc. However, for both cell lines,

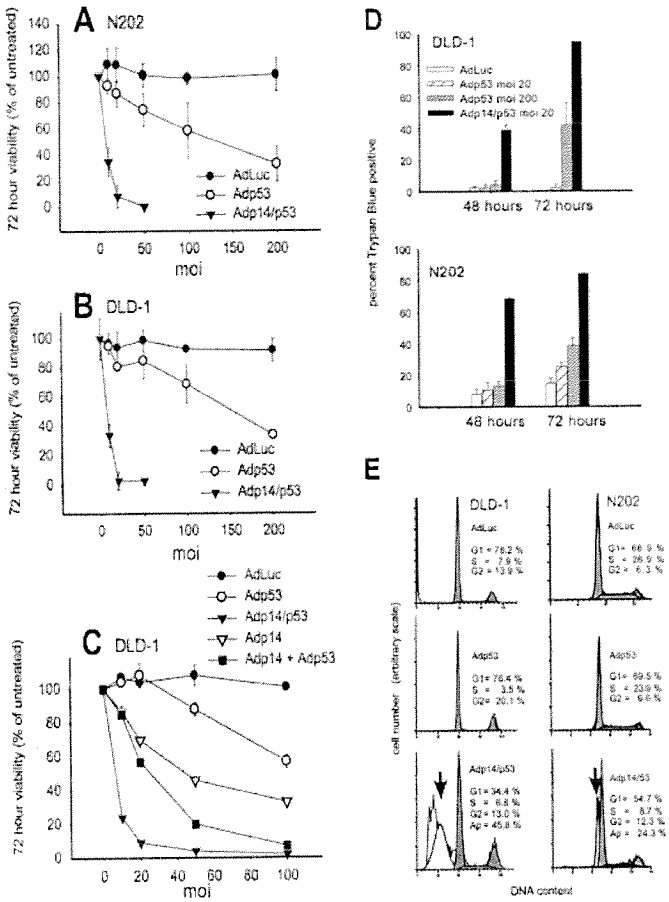


Fig. 2. Percentage of viability measured in 96-well viability assays using (3-(4,5′-dimethylthiazol-2-yl)-5-(3-carboxymethoxylphenyl-2-(4-sulfophenyl)-2H-tetrazolium(3-(4,5′-dimethylthiazol-2-yl)-5-(3-carboxymethoxylphenyl-2-(4-sulfophenyl)-2H-tetrazolium at 72 h after treatment with the indicated doses of AdLuc, Adp53, or Adp14/p53 for DLD-1 (*A*) and N202 (*B*) cells. Each data point represents the average of triplicate samples, with SD shown (for some points, SD are less than the size of symbol). Data are normalized to viability measured in control, untreated wells. *C*, similar assay carried out on DLD-1 cells treated singly with either Adp53 or Adp14 at the indicated doses, or with a combination of the two vectors, each at the indicated dose. *D*, Trypan Blue exclusion assay of DLD-1 and N202 cells 48 and 72 h after treatment with AdLuc, Adp53, or Adp14/p53 at 20 pfu/cell or Adp53 at 200 pfu/cell. Data points represent the average of duplicate wells. *E*, FACS analysis of propidium iodide-stained cells harvested 48 h after treatment with 20 pfu/cell AdLuc, Adp53, or Adp14/p53.

treatment with Adp14/p53 resulted in the accumulation of cells in a subdiploid peak characteristic of cells undergoing apoptosis (Fig. 2*E*, *arrows* in *bottom panels*). The subdiploid fraction of cells accounted for some 42 and 25% of the cell population in DLD-1 and N202 cells, respectively. A second independent analysis gave similar results.

**Adp14/p53 Induces Widespread Apoptosis *in Vivo*.** We used murine N202 cells grown in dorsal skin fold chambers in nude mice to visualize the *in vivo* behavior of cells treated with Adp14/p53, Adp53, or AdLuc (control). Cells were modified with an H2B-GFP fusion protein to facilitate visualization of nuclear changes characteristic of apoptotic or mitotic cells. Unlike human DLD-1 cells and most human tumor lines examined in dorsal skin fold chambers, murine tumor cell lines, such as N202, grow as nonencapsulated tumors more representative of a spontaneous tumor in full contact with its environment,[5] and were therefore used for this study. Cells were treated

[5] G. I. Frost, B. Dudouet, J. Lustgarten, and P. Bogstrom. The roles of epithelial-mesenchymal interactions and the innate immune response on the tumorigenicity of human prostate carcinoma cells grown in immuno-compromised mice, submitted for publication.

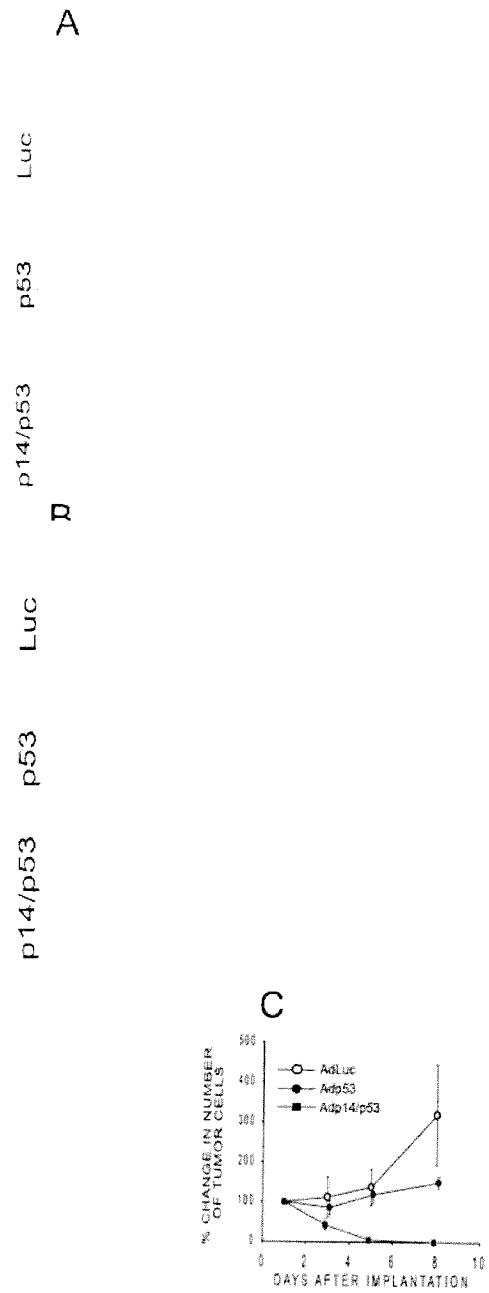


Fig. 3. Photomicrographs illustrating the effects of vector treatment with AdLuc (control), Adp53, or p14/p53 on N202 cells grown in dorsal skin fold chambers in nude mice. *A*, series of photomicrographs at ×20 magnification showing nuclear morphology and cell density changes at 1, 3, 5, and 8 days after implantation of tumor spheroids. Nuclear events are visualized through expression of a histone H2B-GFP. *White bar* in *top right panel* equals 100 μm. *Arrows*, typical apoptotic cells (*Ap*), mitotic figures (*Mi*), and blood vessels (*V*). *Inset*, higher magnification images (×63) of apoptotic or mitotic nuclei. Inset bar represents 5 μm. *B*, series of photomicrographs (×4) obtained with transillumination and RBC enhancement (BG12 filter) for visualization of neovascularization of vector-treated tumor cells at 1, 3, 5, and 8 days after implantation into chambers. In each *row*, images represent the same section of the chamber on successive days. *White bar* in *top right panel* equals 0.5 mm. *C*, graph showing tumor growth over time calculated by integrating the fluorescence intensity throughout the chamber area as described in "Materials and Methods."

with 20 pfu/cell Adp53 or Adp14/p53 followed by preparation of spheroids and implantation into chambers 36 h later. Nuclear morphology (Fig. 3*A*) and neovascularization (Fig. 3*B*) were examined on days 1, 3, 5, and 8 postimplantation. In Fig. 3*A*, large panels at ×20 magnification show representative fields within each chamber, with apoptotic cells (Ap), mitotic cells (Mi), and blood vessels (V) indicated. Insets show representative apoptotic cells (Ap) or mitotic figures (Mi) at ×63 magnification. On day 1 postimplantation, all three spheroid types displayed dying cells with brightly fluorescent condensed or fragmented nuclei characteristic of apoptosis, and overall cell density was low (Fig. 3*A*, *first column*) as is common after the stress of implantation.[6] By day 3, control chambers (AdLuc) showed more diffuse staining indicative of an increased cell mass, and mitotic cells (Mi) were evident (Fig. 3*A*, *top row*). In contrast, there were still numerous apoptotic cells (Ap) in the chambers containing Adp53-treated cells and more in chambers containing Adp14/p53-treated cells (Fig. 3*A*, *middle* and *bottom rows*, respectively). By day 5, control chambers showed additional increases in cell growth (Fig. 3*C*), and neovasculature (V) became evident (Fig. 3*A*, *top row*). Neovasculature was also evident at day 5 in control chambers at ×4 using transillumination (Fig. 3*B*, *top row*) and appeared as a growing network of fine capillaries. Chambers containing Adp53-treated cells began to show increased cell density with fewer apoptotic cells by day 5 (Fig. 3*A*, *middle row*), but there was less neovascularization than in control chambers (Fig. 3*B*, *middle row*). Chambers containing Adp14/p53-treated cells showed few cells remaining by day 5 (Fig. 3*A*, *bottom row*). By day 8, control chambers showed well-established tumors with extensive neovascularization (Figs. 3, *A* and *B*, *top row*). Chambers containing Adp53-treated cells also showed established tumors, and a capillary network indicative of neovascularization had now become evident (Fig. 3, *A* and *B*, *middle row*). In contrast, chambers containing Adp14/p53-treated cells were largely devoid of cells, with those remaining appearing to be apoptotic (Fig. 3*A*, *bottom row*). No neovascularization was evident in these chambers (Fig. 3*B*, *bottom row*). Fig. 3*C* plots the overall tumor growth based on total GFP fluorescence intensity within the chamber, calculated as described in "Materials and Methods." Points represent the averages of four animals, with SD shown.

**Adp14/p53 Is More Efficient than Adp53 at Inducing p53 Target Gene Expression.** We used RT-PCR and Western analysis, respectively, to analyze message and protein expression for mdm2, the cell cycle inhibitor p21waf1, and the pro-apoptotic gene *bax*, all of which have p53-responsive promoters (Fig. 4). We also measured levels of the antiapoptotic bcl2 protein and calculated the ratio of bax to bcl2, which increases in apoptotic cells. Cells were treated with 20 pfu/cell Adp53 or Adp14/p53 to therefore induce equivalent levels of p53 message (Fig. 1*A*). Consistent with the higher levels of induced p53 protein achieved with Adp14/p53 under these conditions (Fig. 1*B*), we observed enhanced transcription of *mdm2*, *p21waf1*, and *bax* in both DLD-1 and N202 cells by RT-PCR analysis after treatment with Adp14/p53 but little or no detectable enhancement of transcription of these genes after similar treatment with Adp53 (Fig. 4*A*). Bars represent averages and SD of triplicate samples after correction for an internal control gene, glyceraldehyde-3-phosphate dehydrogenase (for N202) or actin (DLD-1), and after normalizing to expression levels in AdLuc-treated cells. As shown by the Western blot in Fig. 4*B*, levels of the mdm2, p21waf1, and bax gene products also increased after treatment with Adp14/p53, whereas similar Adp53 treatment resulted in little or no change in expression of these gene products. Additionally shown in Fig. 4*B* are protein levels for bcl2. Digital quantitation of band intensities for bax and bcl2 gave relative bax:bcl2 ratios for AdLuc-, Adp53-, and Adp14/p53-treated cells, respectively, of 1, 1.4, 5.8 (N202), and 1, 0.8, 3.6 (DLD-1). The higher ratio observed for Adp14/p53-treated cells is consistent with the increased apoptotic cell death associated with this treatment (Fig. 2*E*).

[6] P. Borgstrom, unpublished observations.

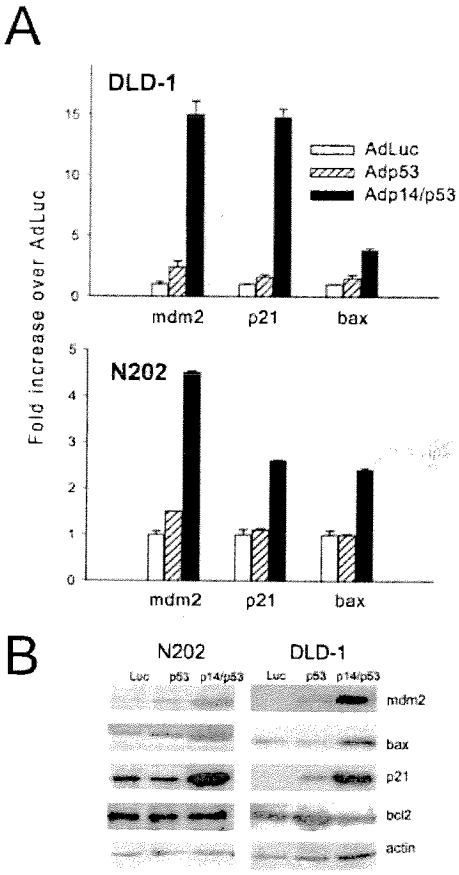


Fig. 4. *A*, semiquantitative RT-PCR and agarose gel electrophoretic analysis of gene expression of p53 downstream target genes *mdm2*, *p21waf1*, and *bax* 48 h after treatment of N202 and DLD-1 cells with 20 pfu/cell AdLuc, Adp53, or Adp14/p53 (4 h). For each gene, linear conditions were established by titrating increasing quantities of cDNA from vector-treated DLD-1 cells. PCR band intensities were quantitated by digital analysis, and bars represent average of triplicate samples, corrected for internal controls [actin (*DLD-1*) or glyceraldehyde-3-phosphate dehydrogenase (*N202*)] and normalized to expression levels in AdLuc-treated cells. *B*, Western analysis of the mdm2, p21waf1, and bax gene products, evaluated 48 h after the same vector treatments as in *A*. Actin expression served as a control. Expression of bcl2 was also evaluated. Each *lane* represents 20 $\mu$g of protein.

## DISCUSSION

In this study, we demonstrate that treatment of tumor cells with a bicistronic adenoviral vector encoding the p14ARF and p53 tumor suppressors (Adp14/p53) can result in complete suppression of tumor cell growth and viability under treatment conditions where a single gene vector for p53 (Adp53) or p14ARF (Adp14) achieves minimal reduction in growth and viability. The bicistronic vector is also more effective than a combination of single gene vectors for p14ARF and p53, possibly because a bicistronic vector will ensure uptake of both genes in targeted cells and will avoid possible interference between two strong promoter activities. Treatment with Adp14/p53 leads to the accumulation of some 13–16-fold higher levels of p53 protein by 48-h post-treatment than is achieved by similar treatment with Adp53 and is accompanied by increased RNA and protein expression of the p53 downstream target genes *p21*, *mdm2*, and *bax* and by an elevated ratio of bax:bcl2 characteristic of cells undergoing apoptosis. Increased cell death after treatment of cells with Ap14/p53 is observed *in vitro* by Trypan Blue exclusion analysis. Increased apoptosis after treatment with Adp14/p53 is observed by FACS cell cycle analysis and *in vivo* by video microscopy of cells growing in dorsal skin fold chambers. Adp14/p53 and Adp53 induce similar levels of p53 message under similar treatment conditions, indicating that post-transcriptional or post-translational mechanisms are responsible for the differences in p53 protein accumulation by the two vectors.

Post-translational control of p53 is known to play a key role in regulating the accumulation and activity of the p53 pathway. A well-studied post-translational control mechanism involves a regulatory feedback loop with mdm2, a ubiquitin ligase that targets the p53 protein for degradation and is itself up-regulated by p53 through transcriptional transactivation (25). Although the feedback loop is unlikely to act on endogenous mutant p53 (DLD-1), where a mutation in the DNA-binding domain (codon 241) changes the conformation of the protein, impairing mdm2 binding and disrupting transcriptional transactivation, the loop will tend to counter any increase in virally expressed wild-type p53 after gene transfer. Although the cell lines we have examined express endogenous p14ARF, which should bind to and oppose the negative regulatory activity of mdm2, endogenous levels of p14ARF are low and appear to be insufficient to ensure maximal accumulation of p53. Simultaneous ectopic expression of p14ARF and p53 may therefore be necessary to promote increased accumulation of wild-type p53 protein (Fig. 1, *A* and *B*).

Consistent with a role for p14ARF in stabilizing p53 through the mdm2/p53 feedback loop, the increased accumulation of p53 protein in cells treated with Adp14/p53 could be accounted for, at least in part, by an increase in p53 protein half-life of some 2.5-fold, from some 4 h to >10 h. In addition to an enhanced stability of the p53 protein in the presence of overexpressed p14ARF, our results point to a novel role for p14ARF in the translational regulation of p53. At equivalent doses of Adp53 and Adp14/p53 (20 pfu/cell), conditions where p53 mRNA expression is the same for the two treatments, we observed a 2-fold higher initial protein synthesis rate for p53 protein after treatment with Adp14/p53, as we did after treatment with Adp53, based on a 1-h radioactive pulse. The effect was also observed with a combination of single gene vectors for p53 and p14ARF (Adp53 + Adp14) and is therefore vector independent and unrelated to possible effects contributed by the internal ribosomal entry site in the bicistronic vector. Differences in total protein synthesis rates could not account for the effects on p53, because total protein synthesis was somewhat reduced in cells treated with Adp14/p53 or Adp14 + Adp53. The fact that treatment of cells with Adp14 together with Ad$\beta$-gal, an adenoviral vector construct similar to Adp53, did not lead to an enhanced protein synthesis rate of the $\beta$-galactosidase gene product indicates that the effect of p14ARF expression on p53 protein synthesis rates was likely to be specific for p53. The observation that bicistronic coexpression of p14ARF and p53 was superior to combination treatments with single gene vectors with regard to growth suppression (Fig. 2*C*) but not overall p53 translation rates (Fig. 1*E*) may be attributable to a more heterogeneous distribution of p14ARF and p53 expression levels after treatment with single gene vectors. Although this heterogeneity could result in a similar enhancement of p53 protein synthesis averaged over the cell population as a whole, as is observed with bicistronic vector treatment, it could nevertheless leave a subset of cells with expression levels of one or the other gene below the threshold level needed to trigger synergistic suppression of cell growth and viability observed with the bicistronic vector, thus accounting for the residual cell viability observed in Fig. 2*C* for the combination vector approach.

Translational regulation of p53 is known to play a role in p53 protein accumulation after DNA damage (26, 27), and its deregulation in some cancers may contribute to the tumor phenotype (28). Translational regulatory sequences in the 3′ and 5′ untranslated regions of *p53* mRNA (26, 29) are absent from the vectors we are using and cannot account for the effects we observe. However, our results could be relevant to studies demonstrating an association between p53, mdm2, and L5 protein, a component of the large ribosomal subunit

(30), and to a recent study revealing a novel role for mdm2 in translational regulation of p53 (3). In particular, mdm2 was observed to promote the translation of p53 through binding to the $NH_2$ terminus of the nascent polysome-associated p53 peptide chain, in addition to its role described previously in promoting the degradation of p53 of full-length p53 (3). Because p14ARF binds to a site on mdm2 (31, 32) distinct from the site on mdm2 that binds p53 (33) and does not prevent binding of mdm2 to p53 (5, 33), it is possible that overexpressed p14ARF contributes to the accumulation of p53 protein by directing mdm2 away from active full-length protein, where it promotes degradation, to sites of p53 synthesis, where it enhances translation. Such a model would predict that endogenous p53 protein might also be subject to translational regulation by p14ARF, and additional studies will be needed to explore this possibility.

The combined treatment with p14 and p53 compared with p53 alone resulted in increased RNA and protein expression of p53 downstream target genes *mdm2, p21waf1,* and *bax,* as expected, as well as with increased apoptosis *in vitro* and *in vivo,* and an elevated ratio of bax:bcl2 expression associated with apoptosis. These increases are consistent with the increased levels of p53 protein achieved with Adp14/p53, compared with Adp53. In addition to its effects on p53, p14ARF may also contribute additional p53-independent tumor suppressor functions, as indicated by several recent studies (19, 34, 35). Although the mechanism of this additional function has not been elucidated, it might involve one or more binding partners for p14ARF other than mdm2. Several of these have been identified and include E2F-1 (36), topoisomerase (37), mdmx (38), and CARF (39). Thus, the superior tumor suppressor activity of the bicistronic vector may derive from both p53-dependent and -independent activities of p14ARF.

The chamber model data suggest that coexpression of p14ARF and p53 may also have greater antitumor activity *in vivo* than does p53 alone, as manifested by inereased apoptosis. Furthermore, angiogenesis, which is critical for tumor growth, was reduced in chambers implanted with ectopic p53-expressing tumor cells and was not observed at all in chambers implanted with ectopic p14ARF + p53-expressing tumor cells. Although a failure to observe angiogenesis could have been, at least in part, a consequence of reduced cell growth, the observations are consistent with several lines of evidence linking p53 and p14ARF expression to reduced angiogenesis. Homozygous deletion of p53 in a human cancer cell line has been observed to promote angiogenesis and tumor growth in nude mice (40). Furthermore, p53 suppresses expression of vascular endothelial growth factor required for vascular growth (41) and induces expression of thrombospondin, an inhibitor of vascular growth (42). p53 also promotes mdm2-mediated degradation of the $\alpha$ subunit of hypoxia-inducible factor 1, which promotes angiogenesis under hypoxic conditions (40). Independently of p53, p14ARF may also inhibit hypoxia-inducible factor-1 by binding to and sequestering it in the nucleolus (43), thereby providing both p53-dependent and -independent components to its antiangiogenic effects. Because of the importance of angiogenesis to tumor growth, numerous antiangiogenic approaches have been considered for cancer treatment. An antiangiogenic component to tumor suppression by Adp14/p53 would amplify the therapeutic efficacy of the vector by creating an environment generally unfavorable for tumor cell proliferation.

Therapeutic applications of the p53 tumor suppressor are already in an advanced stage of clinical development, with numerous clinical trials ongoing or completed that attest to the safety and efficacy of adenovirus-mediated p53 gene transfer in cancer patients (see Ref. 14 for review). The studies reported here suggest that an extension of these approaches to include p14ARF would be feasible and may be more effective than p53 alone. It has been reported previously that certain tumor cells retaining endogenous expression of wild-type p53 but lacking p14ARF can be efficiently suppressed by supplying both p53 and p14ARF (44). In addition, coinfection of tumor cells with a p14ARF and p53 adenovirus has been reported to have a cooperative effect in suppressing tumor cell growth (45). Our present study extends these observations and suggests that bicistronic coexpression of p14ARF and p53 could be superior to single gene treatments, as well as combination treatments with single gene vectors, and could therefore have broad application to cancer treatment by ensuring maximal accumulation of p53 and full restoration of the p53 pathway.

## REFERENCES


1. Wu, X., Bayle, J. H., Olson, D., and Levine, A. J. The p53-mdm-2 autoregulatory feedback loop. Genes Dev., *7:* 1126–1132, 1993.
2. Shieh, S. Y., Ikeda, M., Taya, Y., and Prives, C. DNA damage-induced phosphorylation of p53 alleviates inhibition by MDM2. Cell, *91:* 325–334, 1997.
3. Yin, Y., Stephen, C. W., Luciani, M. G., and Fahraeus, R. p53 Stability and activity is regulated by Mdm2-mediated induction of alternative p53 translation products. Nat. Cell Biol., *4:* 462–467, 2002.
4. Kamijo, T., Weber, J. D., Zambetti, G., Zindy, F., Roussel, M. F., and Sherr, C. J. Functional and physical interactions of the ARF tumor suppressor with p53 and Mdm2. Proc. Natl. Acad. Sci. USA, *95:* 8292–8297, 1998.
5. Zhang, Y., Xiong, Y., and Yarbrough, W. G. ARF promotes MDM2 degradation and stabilizes p53: ARF-INK4a locus deletion impairs both the Rb and p53 tumor suppression pathways. Cell, *92:* 725–734, 1998.
6. Robertson, K. D., and Jones, P. A. The human ARF cell cycle regulatory gene promoter is a CpG island which can be silenced by DNA methylation and down-regulated by wild-type p53. Mol. Cell. Biol., *18:* 6457–6473, 1998.
7. Greenblatt, M. S., Bennett, W. P., Hollstein, M., and Harris, C. C. Mutations in the p53 tumor suppressor gene: clues to cancer etiology and molecular pathogenesis. Cancer Res., *54:* 4855–4878, 1994.
8. Hollstein, M., Sidransky, D., Vogelstein, B., and Harris, C. C. p53 mutations in human cancers. Science, *253:* 49–53, 1991.
9. Kannan, K., Munirajan, A. K., Krishnamurthy, J., Bhuvarahamurthy, V., Mohanprasad, B. K., Panishankar, K. H., Tsuchida, N., and Shanmugam, G. The p16INK4alpha/p19ARF gene mutations are infrequent and are mutually exclusive to p53 mutations in Indian oral squamous cell carcinomas. Int. J. Oncol., *16:* 585–590, 2000.
10. Pinyol, M., Hernandez, L., Martinez, A., Cobo, F., Hernandez, S., Bea, S., Lopez-Guillermo, A., Nayach, I., Palacin, A., Nadal, A., Fernandez, P. L., Montserrat, E., Cardesa, A., and Campo, E. INK4a/ARF locus alterations in human non-Hodgkin's lymphomas mainly occur in tumors with wild-type p53 gene. Am. J. Pathol., *156:* 1987–1996, 2000.
11. Deb, S. P. Function and dysfunction of the human oncoprotein MDM2. Front. Biosci., *7:* d235–d243, 2002.
12. Gjerset, R. A., and Mercola, D. Sensitization of tumors to chemotherapy through gene therapy. Adv. Exp. Med. Biol., *465:* 273–291, 2000.
13. Gjerset, R. A., Turla, S. T., Sobol, R. E., Scalise, J. J., Mercola, D., Collins, H., and Hopkins, P. J. Use of wild-type p53 to achieve complete treatment sensitization of tumor cells expressing endogenous mutant p53. Mol. Carcinog., *14:* 275–285, 1995.
14. Saadatmandi, N., Wilson, D. R., and Gjerset, R. A. p53 gene ther. *In:* J. R. Bertino (ed.), Encyclopedia of Cancer, Vol. 3, pp. 425–441. Amsterdam, New York, Paris: Academic Press, 2002.
15. Fujiwara, T., Grimm, E. A., Mukhopadhyay, T., Zhang, W. W., Owen-Schaub, L. B., and Roth, J. A. Induction of chemosensitivity in human lung cancer cells in vivo by adenovirus-mediated transfer of the wild-type *p53* gene. Cancer Res., *54:* 2287–2291, 1994.
16. Lowe, S. W., Ruley, H. E., Jacks, T., and Housman, D. E. p53-dependent apoptosis modulates the cytotoxicity of anticancer agents. Cell, *74:* 957–967, 1993.
17. Gjerset, R. A., Lebedeva, S., Haghighi, A., Turla, S. T., and Mercola, D. Inhibition of the Jun kinase pathway blocks DNA repair, enhances p53-mediated apoptosis and promotes gene amplification. Cell Growth Differ., *10:* 545–554, 1999.
18. Sacco, M. G., Gribaldo, L., Barbieri, O., Turchi, G., Zucchi, I., Collotta, A., Bagnasco, L., Barone, D., Montagna, C., Villa, A., Marafante, E., and Vezzoni, P. Establishment and characterization of a new mammary adenocarcinoma cell line derived from MMTV neu transgenic mice. Breast Cancer Res. Treat., *47:* 171–180, 1998.
19. Saadatmandi, N., Tyler, T., Huang, Y., Haghighi, A., Frost, G., Borgstrom, P., and Gjerset, R. A. Growth suppression by a p14(ARF) exon 1beta adenovirus in human tumor cell lines of varying p53 and Rb status. Cancer Gene Ther., *9:* 830–839, 2002.
20. Ryan, K. M., Phillips, A. C., and Vousden, K. H. Regulation and function of the p53 tumor suppressor protein. Curr. Opin. Cell Biol., *13:* 332–337, 2001.
21. Gjerset, R. A., Arya, J., Volkman, S., and Haas, M. Association of induction of a fully tumorigenic phenotype in murine radiation-induced T-lymphoma cells with loss of differentiation antigens, gain of CD44, and alterations in p53 protein levels. Mol. Carcinog., *5:* 190–198, 1992.
22. Lehr, H. A., Leunig, M., Menger, M. D., Nolte, D., and Messmer, K. Dorsal skinfold chamber technique for intravital microscopy in nude mice. Am. J. Pathol., *143:* 1055–1062, 1993.

23. Frost, G. I., and Borgstrom, P. Real time in vivo quantitation of tumor angiogenesis. *In:* J. K. B. a. A. A. Adjei (ed.), Methods in Molecular Medicine, Novel Anti-Cancer Drug Protocols, Vol. 85, pp. 65–78. Totowa, NJ: Humana Press, Inc., 2003.
24. Dorigo, O., Turla, S. T., Lebedeva, S., and Gjerset, R. A. Sensitization of rat glioblastoma multiforme to cisplatin in vivo following restoration of wild-type p53 function. J. Neurosurg., *88:* 535–540, 1998.
25. Haupt, Y., Maya, R., Kazaz, A., and Oren, M. Mdm2 promotes the rapid degradation of p53. Nature, *387:* 296–299, 1997.
26. Mosner, J., Munmenbrauer, T., Bauer, C., Sczakiel, G., Grosse, F., and Deppert, W. Negative feedback regulation of wild-type p53 biosynthesis. EMBO J., *14:* 4442–4449, 1995.
27. Fu, L., and Benchimol, S. Participation of the human p53 3′UTR in translational repression and activation following gamma-irradiation. EMBO J., *16:* 4117–4125, 1997.
28. Fu, L., Minden, M. D., and Benchimol, S. Translational regulation of human p53 gene expression. EMBO J., *15:* 4392–4401, 1996.
29. Fu, L., Ma, W., and Benchimol, S. A translation repressor element resides in the 3′ untranslated region of human p53 mRNA. Oncogene, *18:* 6419–6424, 1999.
30. Marechal, V., Elenbaas, B., Piette, J., Nicolas, J. C., and Levine, A. J. The ribosomal L5 protein is associated with mdm-2 and mdm-2-p53 complexes. Mol. Cell. Biol., *14:* 7414–7420, 1994.
31. Weber, J. D., Kuo, M. L., Bothner, B., DiGiammarino, E. L., Kriwacki, R. W., Roussel, M. F., and Sherr, C. J. Cooperative signals governing ARF-mdm2 interaction and nucleolar localization of the complex. Mol. Cell. Biol., *20:* 2517–2528, 2000.
32. Bothner, B., Lewis, W. S., DiGiammarino, E. L., Weber, J. D., Bothner, S. J., and Kriwacki, R. W. Defining the molecular basis of Arf and Hdm2 interactions. J. Mol. Biol., *314:* 263–277, 2001.
33. Kussie, P. H., Gorina, S., Marechal, V., Elenbaas, B., Moreau, J., Levine, A. J., and Pavletich, N. P. Structure of the MDM2 oncoprotein bound to the p53 tumor suppressor transactivation domain. Science, *274:* 948–953, 1996.
34. Weber, J. D., Jeffers, J. R., Rehg, J. E., Randle, D. H., Lozano, G., Roussel, M. F., Sherr, C. J., and Zambetti, G. P. p53-independent functions of the p19(ARF) tumor suppressor. Genes Dev., *14:* 2358–2365, 2000.
35. Tsuji, K., Mizumoto, K., Sudo, H., Kouyama, K., Ogata, E., and Matsuoka, M. p53-independent apoptosis is induced by the p19ARF tumor suppressor. Biochem. Biophys. Res. Commun., *295:* 621–629, 2002.
36. Eymin, B., Karayan, L., Seite, P., Brambilla, C., Brambilla, E., Larsen, C. J., and Gazzeri, S. Human ARF binds E2F1 and inhibits its transcriptional activity. Oncogene, *10:* 1033–1041, 2001.
37. Karayan, L., Riou, J. F., Seite, P., Migeon, J., Cantereau, A., and Larsen, C. J. Human ARF protein interacts with Topoisomerase I and stimulates its activity. Oncogene, *19:* 836–848, 2001.
38. Jackson, M. W., Lindstrom, M. S., and Berberich, S. J. MdmX binding to ARF affects Mdm2 protein stability and p53 transactivation. J. Biol. Chem., *276:* 25336–25341, 2001.
39. Hasan, M. K., Yaguchi, T., Sugihara, T., Kumar, P. K., Taira, K., Reddel, R. R., Kaul, S. C., and Wadhwa, R. CARF is a novel protein that cooperates with mouse p19ARF (human p14ARF) in activating p53. J. Biol. Chem., *277:* 37765–37770, 2002.
40. Ravi, R., Mookerjee, B., Bhujwalla, Z. M., Sutter, C. H., Artemov, D., Zeng, Q., Dillehay, L. E., Madan, A., Semenza, G. L., and Bedi, A. Regulation of tumor angiogenesis by p53-induced degradation of hypoxia- inducible factor 1alpha. Genes Dev., *14:* 34–44, 2000.
41. Pal, S., Datta, K., and Mukhopadhyay, D. Central role of p53 on regulation of vascular permeability factor/vascular endothelial growth factor (VPF/VEGF) expression in mammary carcinoma. Cancer Res., *61:* 6952–6957, 2001.
42. Dameron, K. M., Volpert, O. V., Tainsky, M. A., and Bouck, N. Control of angiogenesis in fibroblasts by p53 regulation of thrombospondin-1. Science, *265:* 1582–1584, 1994.
43. Fatyol, K., and Szalay, A. A. The p14ARF tumor suppressor protein facilitates nucleolar sequestration of hypoxia-inducible factor-1alpha (HIF-1alpha) and inhibits HIF-1- mediated transcription. J. Biol. Chem., *276:* 28421–28429, 2001.
44. Lu, W., Lin, J., and Chen, J. Expression of p14ARF overcomes tumor resistance to p53. Cancer Res., *62:* 1305–1310, 2002.
45. Tango, Y., Fujiwara, T., Itoshima, T., Takata, Y., Katsuda, K., Uno, F., Ohtani, S., Tani, T., Roth, J. A., and Tanaka, N. Adenovirus-mediated p14ARF gene transfer cooperates with Ad5CMV-p53 to induce apoptosis in human cancer cells. Hum. Gene Ther., *13:* 1373–1382, 2002.